Mechanism of processive telomerase catalysis revealed by high-resolution optical tweezers

Eric M. Patrick[1], **Joseph Slivka**[2], **Bramyn Payne**[2], **Matthew J. Comstock**[2,✉], **and Jens C. Schmidt**[1,3,✉]

[1]Institute for Quantitative Health Sciences and Engineering, Michigan State University, East Lansing, MI, U.S.A
[2]Department of Physics and Astronomy, Michigan State University, East Lansing MI, U.S.A
[3]Department of Obstetrics, Gynecology, and Reproductive Biology

Telomerase | Telomere | Optical Tweezers | Single-Molecule Fluorescence | G-quadruplex | Cancer | Aging

Correspondence:
schmi706@msu.edu (Twitter: @jenscs83) and mjcomsto@msu.edu

Telomere maintenance by telomerase is essential for continuous proliferation of human cells and is vital for the survival of stem cells and 90% of cancer cells [1]. Telomerase is a reverse transcriptase composed of telomerase reverse transcriptase (TERT) [2], telomerase RNA (TR) [3], and several accessory proteins [4]. To compensate for telomeric DNA lost during DNA replication, telomerase processively adds GGTTAG repeats to the single-stranded overhangs at chromosome ends by copying the template region within its RNA subunit [5,6]. Between repeat additions, the RNA template must be recycled, which requires disrupting the base-pairing between TR and the substrate DNA [6]. How telomerase remains associated with the substrate DNA during this critical translocation step remains unknown. Here, we demonstrate that stable substrate DNA binding at an anchor site within telomerase facilitates the processive synthesis of telomeric repeats. Using a newly developed single molecule telomerase activity assay utilizing high-resolution optical tweezers, we directly measured stepwise, processive telomerase activity. We found that telomerase tightly associates with its DNA substrate, synthesizing multiple telomeric repeats before releasing them in a single large step. The rate at which product is released from the anchor site closely corresponds to the overall rate of product dissociation from elongating telomerase [7], suggesting that it is a key parameter controlling telomerase processivity. We observed folding of the released product DNA into G-quadruplex structures. Our results provide detailed mechanistic insights into processive telomerase catalysis, a process critical for telomere length maintenance and therefore cancer cell survival [8,9].

To investigate substrate extension by a single telomerase ribonucleoprotein (RNP), we developed a single molecule telomerase activity assay using dual-trap high-resolution optical tweezers (Fig. 1a). Telomerase and its substrate were attached to separate polystyrene beads (Fig. 1b). The connection between the two beads was formed by the association of telomerase with its substrate DNA (Fig. 1a,b). When applying a low constant force (4.0-4.5 pN) to the tether, substrate elongation by telomerase was measured as an increase in distance between the two beads (Fig. 1a). To attach telomerase to the bead, we utilized a 3xFLAG-HaloTag on TERT, modified with biotin (Fig. 1b,c). This tag did not affect telomerase assembly, catalytic activity, processivity, or stimulation by POT1/TPP1 (Fig. 1c,d, Extended Data Fig. 1a-c), indicating that it is fully functional.

Using this experimental approach, we set out to analyze how telomerase processively synthesizes telomeric repeats. If substrate DNA is only bound to telomerase by base-pairing to TR we would expect to observe a sequence of single nucleotide (nt) addition events as a result of RNA template movement (Extended Data Fig. 2a). In contrast, if the substrate also binds to telomerase at a secondary anchor site delaying nascent DNA strand release, extension events of one or more 6 nt telomeric repeats should be observed (Extended Data. Fig. 2b). The existence of an anchor site was hypothesized soon after the identification of telomerase [10-12], and some reports support the presence a secondary DNA binding site within telomerase [13-16]. To monitor telomerase activity, tethers were formed in blank solution lacking nucleotides (Fig. 1a). After assuring that tethers had the expected length and a brief control period, during which no activity was detected (Extended Data Fig. 2c,d), tethers were transferred into the adjacent solution containing nucleotides to initiate telomerase catalysis (Fig. 1a). We observed telomerase activity as a progression of stepwise increases in the tether length (Fig. 1e). The total increase in extension ranged from approximately 20-200 nucleotides (nt, Extended Data Fig. 2e). The observed elongation rates for the majority (56%) of traces ranged from 8-50 nt per minute (Extended Data Fig. 2f), which closely agrees with rates measured in bulk experiments [17,18], indicating that the applied force does not alter telomerase activity. The elongation step sizes were broadly distributed, ranging from 5 nt to > 100 nt with the vast majority (86%) being greater than two telomeric repeats (12 nt, Fig. 2a). This suggests that telomerase binds to the DNA substrate at a secondary site in addition to the TR-substrate base pairing. Our observations provide direct evidence that telomerase processively synthesizes telomeric repeats by stably associating with substrate DNA at an anchor site, allowing multiple repeat-addition cycles to occur prior to product release.

In cancer cells, telomerase is thought to elongate telomeres by 50 nt in a single processive elongation event [19]. Given that the majority of elongation steps (68%) are shorter than

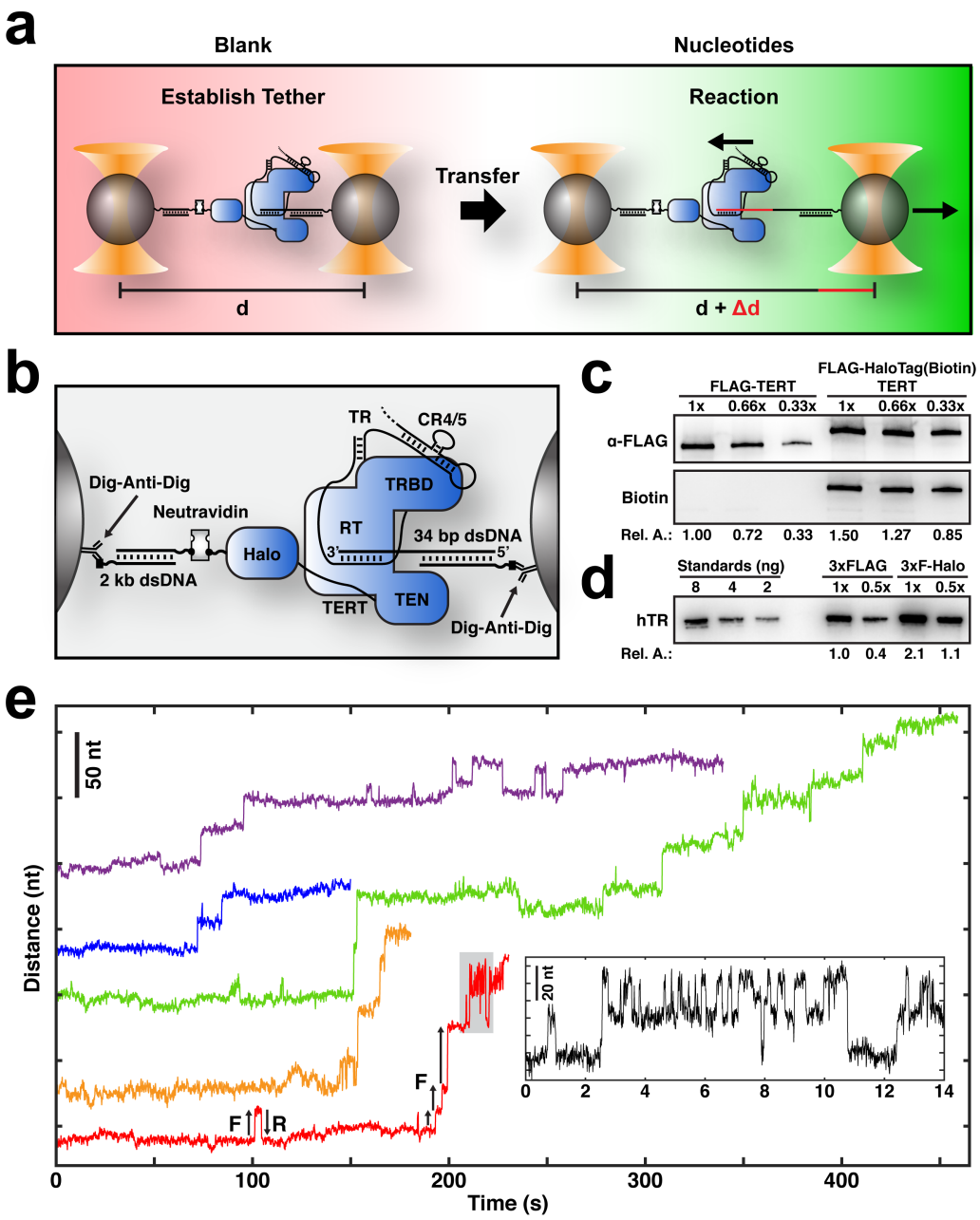

Fig. 1. Direct observation of telomerase catalysis using high-resolution dual-trap optical tweezers. **a**, Experimental design to measure processive telomerase catalysis using dual-optical tweezers. **b**, Schematic showing the molecular details of tether formation to monitor DNA elongation by telomerase. **c**, Western blot of purified 3xFLAG- and 3xFLAG-HaloTag-TERT containing telomerase samples, probed with anti-FLAG-M2-HRP (top) and poly-HRP-streptavidin (bottom). **d**, Northern blot of RNA extracted from purified 3xFLAG- and 3xFLAG-HaloTag-TERT containing telomerase samples, probed with three phosphorylated DNA oligonucleotides complementary to TR. Standards are in vitro transcribed full-length TR. **e**, Representative time trajectories (120 ms per data point) of telomerase catalysis after transfer into nucleotide containing buffer (t = 0) showing processive elongation, forward (F) and reverse (R) stepping. Inset: Zoom-in of region of bottom-most example trace (in red) corresponding to the region shaded gray.

30 nt, this would require multiple anchor site release events prior to complete product dissociation. To determine the global progression of substrate elongation by telomerase we analyzed the transition matrix of all traces (Fig. 2b). The first step of all trajectories was a forward step, after which we observed both increases and decreases in tether length (Fig. 1e, 2a,b). Reverse steps were less frequent than forward steps and, unlike tether extensions, never exceeded 40 nt in length (Fig. 2a,b). Smaller reverse steps frequently matched the preceding forward step and occasionally repetitive forward-reverse step cycling was observed (Fig. 2b). On average, telomerase elongated substrates by approximately 72 nucleotides during the first five state transitions (Fig. 2c). After this initial elongation, the average tether length remained constant from step 6 to 10 (Fig. 2c). This lack of further extension coincided with an increased frequency of reverse steps and the appearance of peaks in the step size distribution at approximately 15 nucleotides in both forward and reverse directions (Fig. 2c,d). These observations demonstrate that telomerase can undergo multiple rounds of DNA

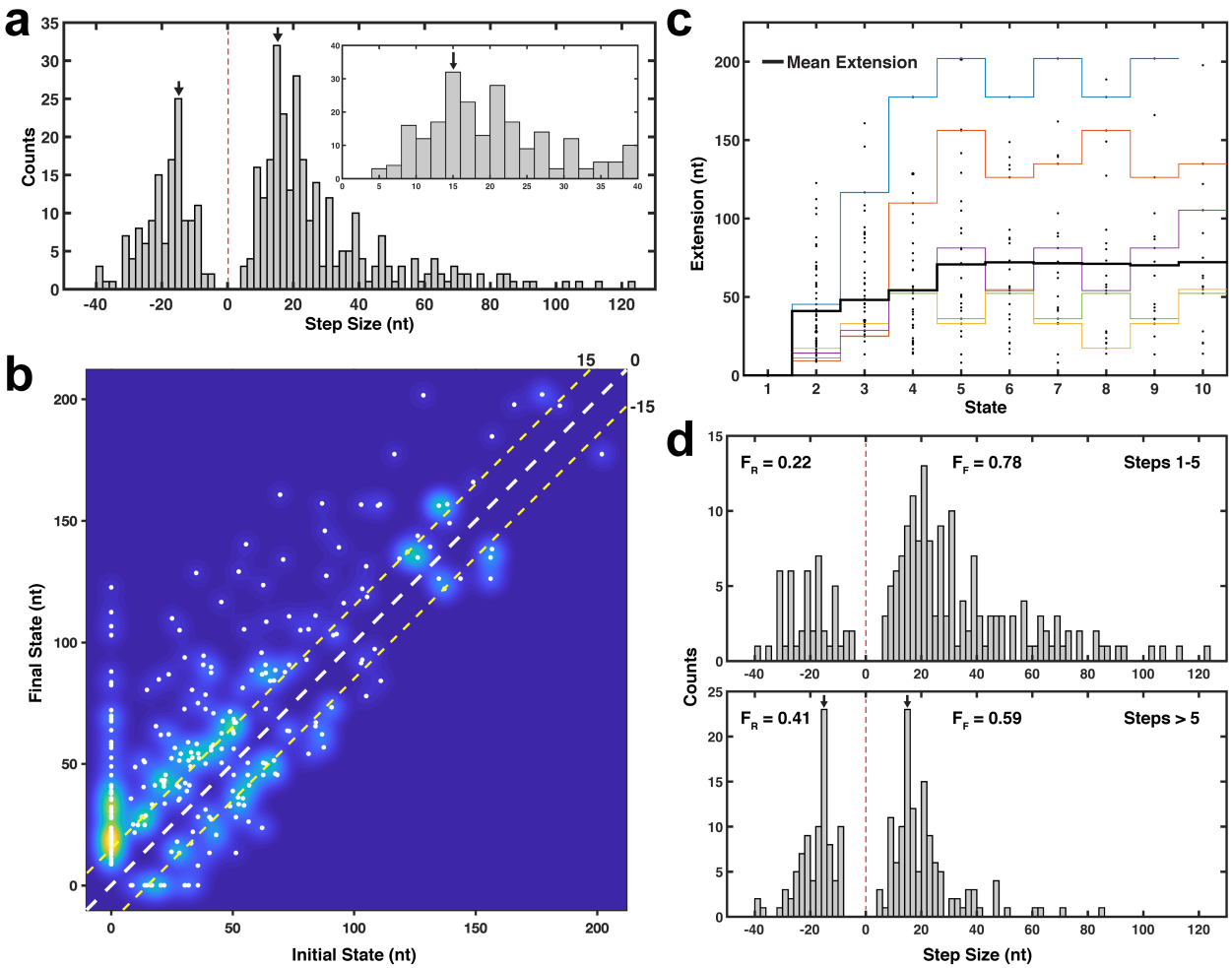

Fig. 2. Telomerase releases multiple telomeric repeats in a single step. **a**, Distribution of the observed tether elongation step sizes of telomerase trajectories (n = 60 distinct tethers, 417 steps total). Inset: zoom-in around the forward step distribution peak. Arrows mark a 15 nt magnitude step size which is the expected GQ folding and unfolding step size. **b**, Kernel density plot of final vs. initial states associated with each step in **a**. The diagonal dashed white line is a guide dividing forward (above line) vs. reverse (below line) steps. The upper and lower dashed yellow lines are guides indicating 15 nt steps forward vs reverse respectively. **c**, Dot plot of the extension for the first 10 states of all telomerase trajectories (n = 60), including the mean extension (black) and individual trajectories (color). **d**, Distribution of step sizes for the first 5 steps (top) and all subsequent steps (bottom) for all trajectories (n = 60 tethers, 417 steps). Arrows mark a 15 nt magnitude step size. F_F and F_R indicate fractions of forward and reverse steps, respectively.

release from the anchor site without complete product dissociation.

We next sought to determine the molecular mechanisms that underlie the reverse steps observed in telomerase catalysis trajectories. Reverse steps could be the consequence of two distinct processes: 1) Rebinding of the product to the anchor site, or 2) folding of product into a G-quadruplex (GQ) structure, which has been shown to affect telomerase catalysis [20]. The most common reverse step size is approximately 15 nt (Fig. 2a,d), which is approximately the expected change in extension for a single GQ folding event under the experimental conditions (Extended Data Fig. 3e) [21]. To test whether GQ folding is responsible for the reverse steps, we conducted telomerase extension experiments in the presence of lithium chloride. Unlike potassium, lithium cations do not support GQ formation [22]. In the presence of lithium, we observed similar processive telomerase extension, including reverse steps (Extended Data Fig. 3a). The overall extension rate was slightly reduced, consistent with bulk experiments (Extended Data Fig. 3b) [20]. However, lithium eliminated the peaks centered at 15 nt in the step size distribution in both the forward and reverse directions (Fig. 2a, Extended Data Fig. 3c,d, arrows), consistent with the interpretation that GQ dynamics are the molecular mechanism underlying these length changes. The remaining reverse steps likely stem from rebinding of the anchor site to product DNA.

To verify that GQ folding and unfolding occurs with the predicted step size of 15 nt and on time scales relevant for our experiments, we performed tweezers experiments tethering GQ sequences without telomerase. Single stranded DNA (ssDNA) sequences capable of forming either single or multiple GQ structures dynamically folded and unfolded with step sizes of 17.6±0.4 nt and 17.5±0.2 nt, respectively (Fig. 3a-d). Occasionally, smaller steps (8 nt) were observed (e.g., Fig. 3c at t = 150 s), which may represent misfolded GQs, or GQs transiently interacting with the tether handles. Förster resonance energy transfer measurements [23] confirmed that folding of the ssDNA was responsible for the observed length

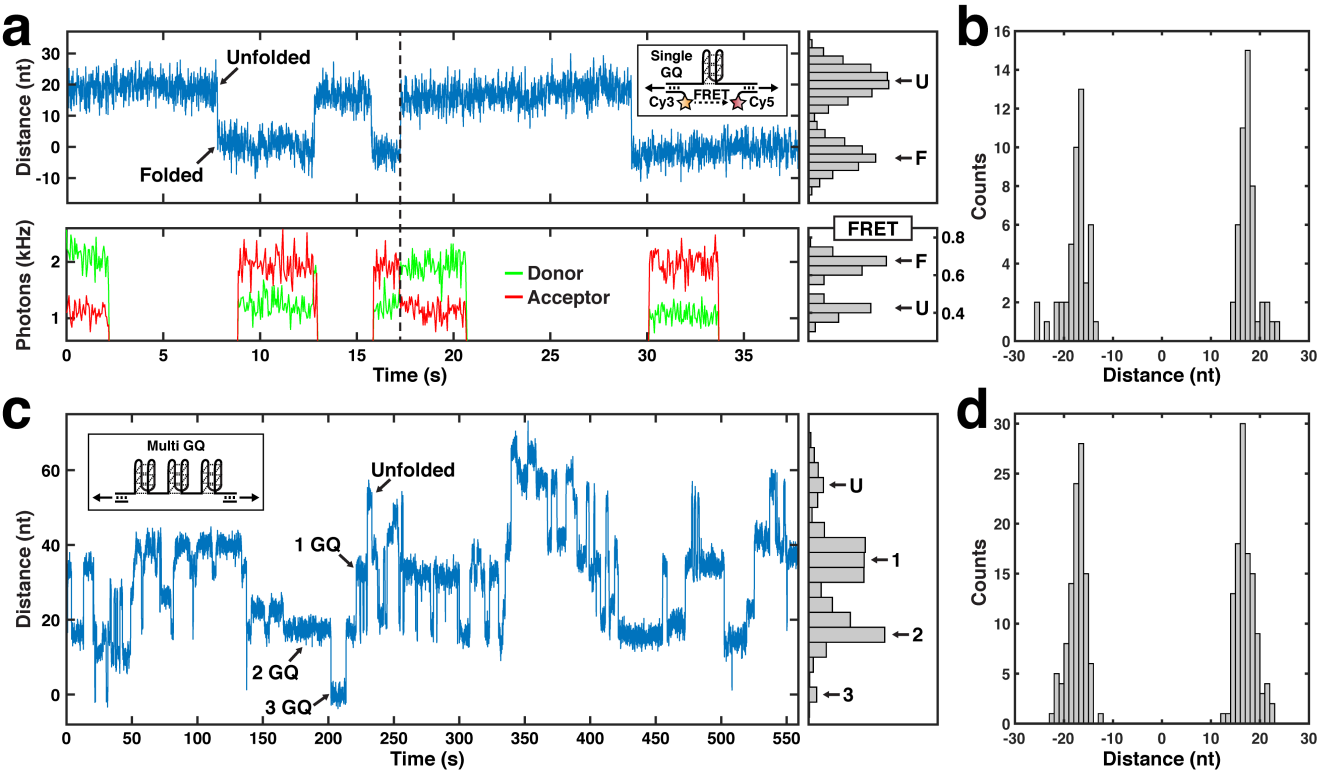

Fig. 3. Single stranded telomeric repeat DNA dynamically folds into G-quadruplex structures. **a**, Representative time trajectory and histogram of the folding dynamics of telomeric repeat ssDNA capable of forming a single GQ, showing trap distance (top, 12 ms per data point) and FRET measurements (bottom, 50 ms per data point). The excitation laser for the FRET donor (Cy3) was only turned on during the time periods for which data are shown. **b**, Step size distribution of folding and unfolding events observed in single GQ tethers (n = 9 tethers, 96 steps). **c**, Representative time trajectory and histogram of the folding dynamics of telomeric repeat ssDNA capable of forming up to three GQs (60 ms per data point). d, Step size distribution of folding and unfolding events observed in multi GQ tethers (n = 5 tethers, 221 steps).

changes (Fig. 3a). For the single GQ tethers, the folding dwell time distribution was a single exponential (τ_f=13.6±1.4 s), while unfolding distributions could only be fit by a sum of a minimum of three exponentials, consistent with the formation of various GQ conformations with distinct stabilities (Extended Data Fig. 4a,b). Both force-extension, and force-feedback measurements confirmed the presence of up to three GQs in the extended telomeric ssDNA sequence (Fig. 3c, Extended Data Fig. 4c). Similar to the single GQ unfolding, the distribution of all dwells for the multi-GQ was fit by a minimum of three exponentials (Extended Data Fig. 4d). These results demonstrate that GQs can rapidly fold and unfold under our experimental conditions. In addition, the step sizes of GQ dynamics largely overlapped with the predicted length change for GQ formation. In total, our results are consistent with the interpretation that both GQ folding and unfolding occurs in product ssDNA that is released from telomerase. Previously, GQs have been thought of as very stable structures that do not unfold unless significant force (> 20 pN) is applied [24,25]. In agreement with observations made by others [26], our results suggest that GQs dynamically fold and unfold, especially when many G-rich repeats are present, which is the physiologically relevant context for telomeric DNA.

The affinity of telomerase for substrate DNA is a key contributing factor to processive telomere repeat synthesis [27]. To determine the affinity of ssDNA for the telomerase anchor site, we analyzed the dwell times prior to the first elongation step of all telomerase trajectories. Since product release is a pre-requisite for the observation of the initial tether extension, this dwell time should reflect the dissociation rate of ssDNA from the telomerase anchor site. Consistent with this hypothesis, the dwell time distribution prior to the first step was well fit by a single exponential decay with a time constant of 97±12 s (Fig. 4a). After the initial extension step, telomerase could exist in at least two configurations: telomerase RNPs with released ssDNA that is either unfolded or folded into a GQ (Fig. 4c). Indeed, the dwell time distributions for the second and third steps fit to the sum of two exponentials (Extended Data Fig. 5a,b). The slow time constants for the second and third steps (77±20 s, 61±13 s, weights 38±9%, 30±9%) were comparable in length to anchor site release. The fast time constants were approximately 30-fold lower (2.1±0.5 s, 1.4±0.3 s, weights 62±8%, 70±9%), indicating that a second, more rapid, process is occurring in addition to anchor site release. Analysis of the dwell times across the first 10 transitions of all trajectories revealed a gradual decrease of the mean dwell time from approximately 95 s to 10 s from steps 1 to 5 (Fig. 4b). The mean dwell time remained constant from steps 5 to 10 (Fig. 4b). The reduction in dwell time to approximately 10 s is concomitant with the increased frequency of reverse steps (Fig. 2c,d) and is comparable to the mean dwell time of GQ folding/unfolding (6.5 s, multi-GQ, Extended Data, Fig. 4d). Together, these observations suggest that GQ folding/unfolding is the molecular

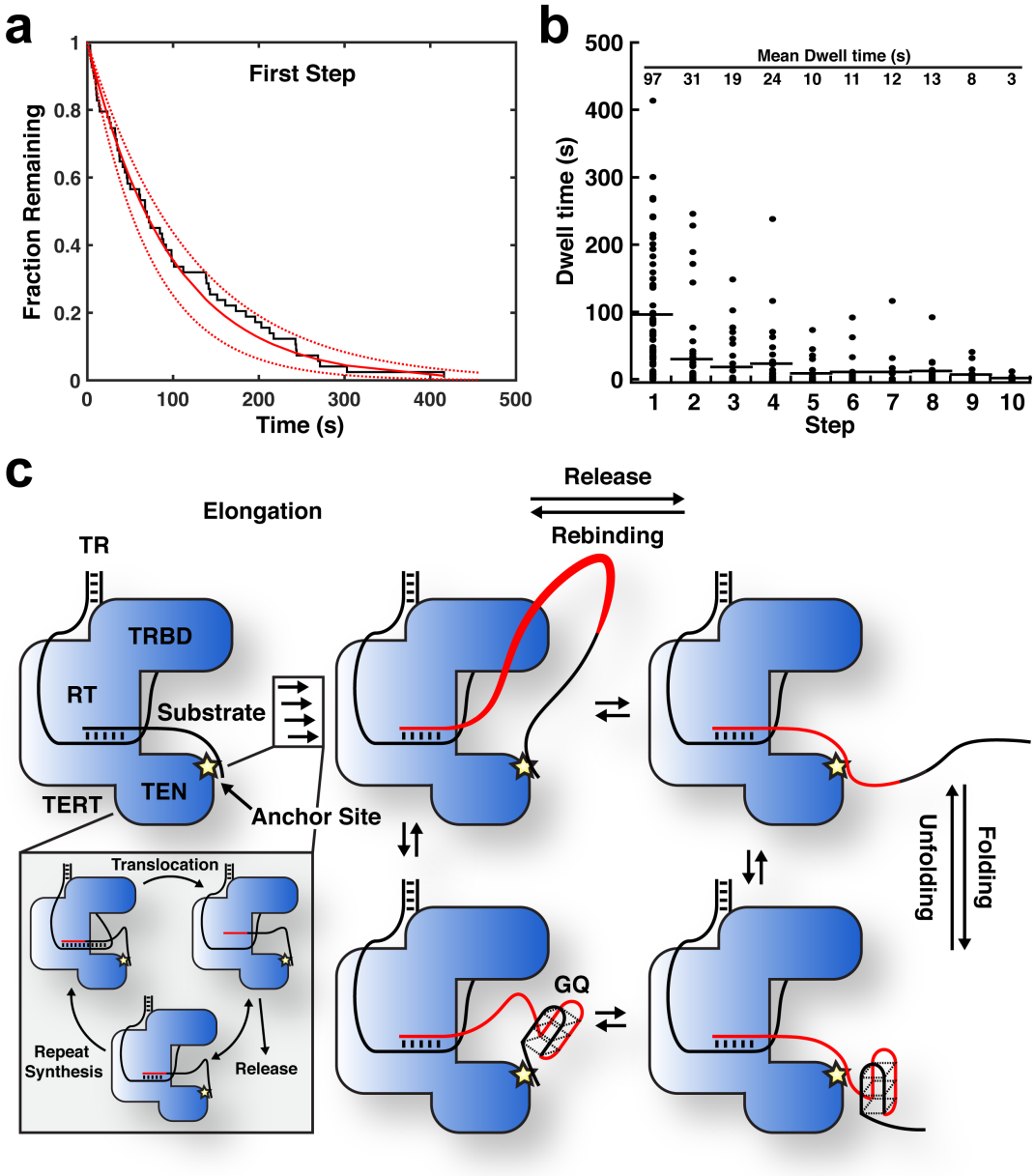

Fig. 4. Dissociation from the anchor site controls product release by telomerase. **a**, Inverse cumulative distribution of dwell times for the first step of all telomerase trajectories (black staircase, n = 60 traces). Solid red line indicates a single exponential fit, dashed lines the 90% confidence intervals. **b**, Dot plot of individual dwell times for the first 10 steps of all telomerase trajectories (n = 60). Mean dwell time is indicated at the top of the graph and by the black horizontal lines. **c**, Model of processive telomere elongation by telomerase (discussed in detail in the text).

process underlying the faster rate in tether length changes. Importantly, the time constant of anchor site release (97 s) is comparable to the time constant of substrate dissociation from elongating telomerase when dGTP concentrations are low (87 s) 7. When dGTP is limiting, the initiation of repeat synthesis after translocation is slow (Fig. 4c, inset) [18]. Thus, telomerase is "stuck" with minimal base-pairing and the anchor site is especially important to prevent substrate dissociation (Fig. 4c, inset). The close correspondence of anchor site and overall substrate dissociation rates suggests that anchor site release is the rate limiting step for substrate dissociation from telomerase.

Together, our direct observation of telomerase catalysis using high- resolution optical tweezers reveals fundamental principles of the molecular mechanisms by which human telomerase processively elongates DNA (Fig. 4c), a process critical for telomere length maintenance [8,9]. Telomerase contains a secondary substrate binding site to prevent premature dissociation from the chromosome end. Future studies will have to address how the anchor site cooperates with POT1/TPP1 to facilitate processive telomere elongation in human cells. Our findings represent an important advance in our understanding of telomere maintenance by telomerase, a cellular process that plays a central role in human aging, as well as cancer formation and survival [1].

ACKNOWLEDGEMENTS
We thank Jayakrishnan Nandakumar and Iain Cheeseman for comments on the manuscript. This work was support by grants from the NSF (MCB-1919439) to M.J.C. and the NIH (R00 GM120386) to J.C.S. J.C.S. is a Damon Runyon Dale F. Frey Scientist supported (in part) by the Damon Runyon Cancer Research Foundation (DFS-24-17). This preprint was generated using a template from Ricardo Henriques.

AUTHOR CONTRIBUTIONS
Experiments were designed by E.M.P., M.J.C., and J.C.S. Optical trapping with telomerase was carried out by E.M.P. Optical trapping with multi G-quadruplex construct was carried out by E.M.P. Optical trapping with single G-quadruplex construct was carried out by J.S. and B.P. All other sample preparation and experiments were carried out by E.M.P. and J.C.S. E.M.P., M.J.C., and J.C.S. analyzed data and wrote the manuscript.

COMPETING INTERESTS
The authors declare no competing interests.

Methods

Telomerase expression and purification. Telomerase was expressed in HEK293T cells as previously described 28. 30x10^6 cells were transfected with 15 µg of TERT plasmid (3xFLAG- or 3xFLAG-HaloTag-TERT) and 60 µg of pSUPER-hTR using 150 µl of Lipofectamine 2000 (Invitrogen) in a total volume of 7.5 ml of OPTI-MEM (Gibco). Cells were harvested and lysed with CHAPS buffer (10 mM TRIS-HCl pH 7.5, 1 mM $MgCl_2$, 1 mM EGTA, 0.5% CHAPS, 10% glycerol, 5 mM beta-mercapto-ethanol) 48 hours after transfection (100x10^6 cells). Telomerase was bound to Anti-FLAG-M2 affinity gel (Sigma-Aldrich, A2220, 100 µl of resin), washed three times with washing buffer (20 mM HEPES pH 7.9, 300 mM KCl, 2 mM $MgCl_2$, 1 mM EDTA, 1 mM DTT, 1 mM PMSF, 0,1% Triton X-100, 10% glycerol), and eluted with 200 µl of wash buffer supplemented with 0.15 mg/ml 3xFLAG peptide (Sigma-Aldrich). Telomerase quantity, composition, assembly, and biotin modification was assessed with western and northern blots as previously described [9], using TR probes 1, 2, and 3 (IDT, Table S1), and antibodies against FLAG (Sigma-Aldrich, anti-FLAG-M2), TCAB1 (Proteintech, 14761-1-AP), dyskerin (Santa Cruz, sc-373956), and poly-HRP-streptavidin (Thermo Scientific. 21140). TR standards for northern blots were in vitro transcribed from PCR products using the HiScribe™ T7 high yield RNA synthesis kit (New England Biolabs). Band intensities were quantified using ImageQuant TL 8.2 (GE Healthcare Life Sciences).

Direct telomerase primer elongation assay. Telomerase activity assays were carried out for 1 hour at 30 °C as previously described in reaction buffer (50 mM TRIS-HCl pH 8.0, 50 mM or 150 mM KCl, 1 mM $MgCl_2$) [29]. Assays with telomerase alone were carried out with 50 nM primer A, 50 mM KCl, 10 µM or 50 µM dATP, dTTP, and dGTP, and 0.33 µM dGTP [α-32P] (Perkin Elmer). Telomerase assays to assess POT1/TPP1 stimulation were carried out with 50 nM primer A5, 150 mM KCl, 100 nM POT1/TPP1, 500 µM dATP, dTTP, 3.3 µM dGTP, and 0.33 µM dGTP [α-32P] (Perkin Elmer). POT1/TPP1 was purified as previously described [30]. Telomerase products were separated on 12% poly-acrylamide, 1xTBE, 7 M Urea, sequencing gels and detected using storage phosphor screens (GE Healthcare Life Sciences, BAS-IP MS 3543) and an Amersham Typhoon IP (GE Healthcare Life Sciences). Phosphorylated primer A-2 was used as a loading control. Activity was quantified as total radioactive incorporated per lane normalized to the loading control. To compare activity between 3xFLAG- and 3xFLAG-HaloTag containing telomerase, specific activity was calculated by dividing the activity measured by telomerase assays by the TR levels determined by northern blot. Processivity was quantified as the intensity of products longer than 6 repeats divided by the total signal per lane.

Optical trapping measurements. All optical trapping measurements were carried out at 23 °C. Optical trapping was carried out using a home-built timeshared dual optical trap combined with confocal single molecule fluorescence microscope instrument as previously described in detail [23,31,32]. Briefly, an acousto-optic modulator (AOM) deflected a 1,064 nm laser (IPG) between two positions to create two independent optical traps (66.7 kHz modulation rate). A PID (proportional-integral-derivative) feedback loop stabilized the trap laser intensity to maintain constant trap stiffness (0.2-0.3 pN/nm) during trap positioning. Bead positions were measured at 66.7 kHz sampling rate using the transmitted trap laser light by infrared-enhanced quadrant photodiodes (Pacific Silicon Devices) via the standard back focal plane interferometry method. Bead position and trap stiffness calibrations were performed via standard fitting of the bead Brownian motion power spectra. A 532 nm fluorescence excitation laser was coaligned between the dual traps at the center of the tether and interlaced with a second AOM to be on only during trap laser off intervals. Fluorescence emission was collected confocally and split by color into standard donor (Cy3) and acceptor (Cy5) emission channels and detected by a pair of single photon counting avalanche photodiodes (APD). Instrument control and data acquisition were performed using a field programmable gate array-based PC card system (National Instruments PCIe-7852R). Instrument control software was written in LabVIEW version 2012 (National Instruments).

The substrate handle (SH) was generated by annealing the substrate handle oligo- nucleotides 1 and 2 (IDT, Table S1). The biotin-digoxigenin handle (BDH) was generate by PCR using biotin and digoxygenin modified oligos 1 and 2 (IDT, Table S1) and pBR322 as template. To establish tethers, the telomerase-substrate complex was formed by incubating 3xFLAG-HaloTag(biotin)-TERT containing telomerase with the SH for 30 minutes at room temperature, prior to binding of the complex to 1 µM diameter polystyrene beads (Spherotech) functionalized with an anti-digoxigenin antibody (Roche) for 10 minutes at room temperature. The BDH was incubated with a 50-fold excess of neutravidin (Thermo Scientific) for 10 minutes at room temperature, prior to binding to anti-digoxigenin antibody modified polystyrene beads 33. Tethers were formed by holding the beads close together in telomerase reaction buffer lacking nucleotides (50 mM TRIS-HCl pH 8.0, 50 mM KCl, 1 mM $MgCl_2$, 1% glucose, 1 mg/ml glucose oxidase, 0.13 mg/ml catalase, 1 mg/ml Trolox) under continuous laminar flow in a multi-channel

home-made chamber 34 to establish the linkage between the neutravidin on the BDH and the biotin-modified 3xFLAG-HaloTag-TERT telomerase. Stable tethers were subjected to force-extension measurements at a ramp rate of 100 nm s^{-1}, which were fit to worm-like chain model DNA polymer modelling parameters. Measurements of telomerase catalysis were initiated in blank buffer. After a control period of approximately 30 seconds, tethers were transferred into reaction buffer supplemented with 50 µM dATP, dTTP, and dGTP. To determine the contribution of G-quadruplex folding and unfolding on product extension by telomerase, trapping experiments were carried out in buffers containing 50 mM LiCl instead of KCl.

To analyze GQ folding and unfolding G-quadruplex forming oligos $GGG(TTAGGG)_3$ and $(TTAGGG)_{12}$ were purchased from IDT (Table S1). GQ constructs were generated by ligating the oligos to DNA handles amplified from Lambda DNA and digested with TspRI (right handle, RH) and pBR322 digested with HindIII or PspGI to make the left handle (LH). The RH and LH were amplified using primers modified with digoxygenin and biotin, respectively (Table S1). FRET donor and acceptor fluorophores flanking the single GQ sequence were added by annealing and ligating Cy3 and Cy5 labeled 9 nt long oligos to complimentary sequences flanking the GQ sequence. The GQ construct was incubated with the streptavidin coated beads (Spherotech) for 1 hour and tethers were formed in situ by establishing a digoxigenin-anti-digoxigenin linkage of the RH with anti-digoxygenin antibody coated beads. Stable tethers were first subjected to force extension at 100 nm s^{-1} spanning a force range from 0-30 pN to unfold any pre-existing structures and to assess tether quality. The trap distance was then set to apply a constant force of 4-4.5 pN and measurements were carried in force-feedback mode.

Template elongation and GQ-dynamics were monitored as a change extension in the tether length by tracking the bead position within the movable trap. The optical trap was operated under active force feedback, where bead positions within the traps were monitored and kept constant by adjusting the location of one trap, thereby applying a constant force of 4 - 4.5 pN to the tether. The recorded motion of the trap tracked the changing extension of the tether e.g., the elongation activity of telomerase, release and rebinding of product, folding and unfolding of GQ structures etc. The change in location of the trap was calibrated to the equivalent change in the number of tether ssDNA nucleotides (nt, e.g., due to the catalytic elongation of the tethered DNA substrate) via standard ssDNA polymer modeling (via the extensible freely jointed chain model, persistence length = 0.75 nm, contour length = 0.56 nm/nt, stretch modulus = 800 pN). Force extension were carried out at 100 nm s^{-1}. The models for tether extension vs force are produced by the sum of the standard polymer models of dsDNA representing the handles (extensible worm-like chain model, persistence length = 53 nm, contour length = 0.34 nm/bp, stretch modulus = 1200 pN) and the relevant quantity of ssDNA [35-37].

Data Analysis. Offline data analysis was performed using standard methods implemented via custom codes programmed in MATLAB version 2018b (Mathworks). Data collected at 66.7 kHz was boxcar averaged to a final lower rate, as specified, but generally sufficiently fast to accurately determine telomerase template elongation states and lifetimes, between 1 and 20 ms per data point. Automatic state and step finding in telomerase trajectories was carried out using the code XL-ICON which is an implementation of the infinite Hidden Markov Modelling (iHMM) method which is a Bayesian nonparametric extension of the very commonly used HMM method and allows for state discovery with simultaneous correction for high-resolution tweezers measurement drift and finite response time [38]. Regions of a small number of traces (4 out of 60) were excluded from contributing to the state and step size distributions because they had a very large number of reversing states that would have obscured the contributions from the remainder of traces. Overall extension rate was calculated by dividing the maximal extension of each trace by the time point at which it was first observed. Step finding for GQ trajectories was carried out in a simpler manner by plotting the first derivative of the trap position. Steps positions were identified as peaks in the derivative that exceeded the cutoff of ±3.5 nm. Step size measurement accuracy was improved by only considering steps whose initial and final states were at least 0.5 s in duration. All trajectories were manually inspected for accuracy of the automated state and step finding. Step sizes in nm were converted to nucleotides using the force dependent extension based on the freely jointed chain model using the same parameters as above. For dwell time analysis, fitting was never performed on binned data. For dwell time distributions well fit by single exponentials, the mean dwell time, which is the maximum likelihood estimator for the time constant, is reported along with the standard error of the mean to estimate uncertainty. For dwell time distributions that were well fit by the sum of two or three exponentials (e.g., the unfolding of the single GQ tether and the distribution of all multi-GQ state dwell times), fitting was performed by minimizing the least squares error in the dwell time cumulative distribution. Error was estimated by finding fit parameter one sigma (68%) confidence bounds by standard bootstrapping of the fitting using resampled data with replacement.

Data Availability. All data generated or analyzed during this study are included in this manuscript (and its supplemental information). Reagents and raw data are available from J.C.S. and M.J.C. upon request.

Computer Code. Custom MATLAB code used to analyze the data generated in this study is available from M.J.C. upon request.

References

1. Stewart, S. A. Weinberg, R. A. Telomeres: cancer to human aging. Annu Rev Cell Dev Biol 22, 531–557 (2006).
2. Nakamura, T. M. et al. Telomerase catalytic subunit homologs from fission yeast and human. Science 277, 955–959 (1997).

3. Feng, J. et al. The RNA component of human telomerase. Science 269, 1236–1241 (1995).
4. Blackburn, E. H. Collins, K. Telomerase: an RNP enzyme synthesizes DNA. Cold Spring Harb Perspect Biol 3, (2011).
5. Greider, C. W. Telomerase is processive. Mol. Cell. Biol. 11, 4572–4580 (1991).
6. Wu, R. A., Upton, H. E., Vogan, J. M. Collins, K. Telomerase Mechanism of Telomere Synthesis. Annu. Rev. Biochem. 86, 439–460 (2017).
7. Dalby, A. B., Hofr, C. Cech, T. R. Contributions of the TEL-patch Amino Acid Cluster on TPP1 to Telomeric DNA Synthesis by Human Telomerase. J Mol Biol 427, 1291–1303 (2015).
8. Wu, R. A., Tam, J. Collins, K. DNA-binding determinants and cellular thresholds for human telomerase repeat addition processivity. EMBO J 36, 1908–1927 (2017).
9. Schmidt, J. C., Zaug, A. J., Kufer, R. Cech, T. R. Dynamics of human telomerase recruitment depend on template-telomere base pairing. Mol Biol Cell 29, 869–880 (2018).
10. Greider, C. W. Blackburn, E. H. Identification of a specific telomere terminal transferase activity in Tetrahymena extracts. Cell 43, 405–413 (1985).
11. Morin, G. B. Recognition of a chromosome truncation site associated with alpha-thalassaemia by human telomerase. Nature 353, 454–456 (1991).
12. Collins, K. Greider, C. W. Tetrahymena telomerase catalyzes nucleolytic cleavage and nonprocessive elongation. Genes Dev 7, 1364–1376 (1993).
13. Robart, A. R. Collins, K. Human telomerase domain interactions capture DNA for TEN domain-dependent processive elongation. Mol Cell 42, 308–318 (2011).
14. Jacobs, S. A., Podell, E. R. Cech, T. R. Crystal structure of the essential N-terminal domain of telomerase reverse transcriptase. Nat Struct Mol Biol 13, 218–225 (2006).
15. Lue, N. F. A Physical and Functional Constituent of Telomerase Anchor Site. J Biol Chem 280, 26586–26591 (2005).
16. Akiyama, B. M., Parks, J. W. Stone, M. D. The telomerase essential N-terminal domain promotes DNA synthesis by stabilizing short RNA–DNA hybrids. Nucleic Acids Res 43, 5537–5549 (2015).
17. Xi, L. Cech, T. R. Inventory of telomerase components in human cells reveals multiple subpopulations of hTR and hTERT. Nucleic Acids Res 42, 8565–8577 (2014).
18. Chen, Y., Podlevsky, J. D., Logeswaran, D. Chen, J. J.-L. A single nucleotide incorporation step limits human telomerase repeat addition activity. EMBO J 37, e97953 (2018).
19. Zhao, Y. et al. Telomere extension occurs at most chromosome ends and is uncoupled from fill-in in human cancer cells. Cell 138, 463–475 (2009).
20. Jansson, L. I. et al. Telomere DNA G-quadruplex folding within actively extending human telomerase. Proceedings of the National Academy of Sciences 116, 9350–9359 (2019).
21. Phan, A. T. Human telomeric G-quadruplex: structures of DNA and RNA sequences. FEBS J. 277, 1107–1117 (2010).
22. Sen, D. Gilbert, W. A sodium-potassium switch in the formation of four-stranded G4-DNA. Nature 344, 410–414 (1990).
23. Comstock, M. J., Ha, T. Chemla, Y. R. Ultrahigh-resolution optical trap with single-fluorophore sensitivity. Nat Meth 8, 335–340 (2011).
24. Mitra, J. et al. Extreme mechanical diversity of human telomeric DNA revealed by fluorescence-force spectroscopy. Proceedings of the National Academy of Sciences 116, 8350–8359 (2019).
25. Abraham Punnoose, J. et al. Random Formation of G-Quadruplexes in the Full-Length Human Telomere Overhangs Leads to a Kinetic Folding Pattern with Targetable Vacant G-Tracts. Biochemistry 57, 6946–6955 (2018).
26. Hwang, H. et al. Telomeric overhang length determines structural dynamics and accessibility to telomerase and ALT-associated proteins. Structure 22, 842–853 (2014).
27. Latrick, C. M. Cech, T. R. POT1-TPP1 enhances telomerase processivity by slowing primer dissociation and aiding translocation. EMBO J 29, 924–933 (2010).
28. Sauerwald, A. et al. Structure of active dimeric human telomerase. Nat Struct Mol Biol 20, 454–460 (2013).
29. Zaug, A. J., Crary, S. M., Jesse Fioravanti, M., Campbell, K. Cech, T. R. Many disease-associated variants of hTERT retain high telomerase enzymatic activity. Nucleic Acids Res 41, 8969–8978 (2013).
30. Schmidt, J. C., Dalby, A. B. Cech, T. R. Identification of human TERT elements necessary for telomerase recruitment to telomeres. Elife 3, e03563 (2014).
31. Whitley, K. D., Comstock, M. J. Chemla, Y. R. High-Resolution 'Fleezers': Dual-Trap Optical Tweezers Combined with Single-Molecule Fluorescence Detection. Methods Mol. Biol. 1486, 183–256 (2017).
32. Whitley, K. D., Comstock, M. J. Chemla, Y. R. High-Resolution Optical Tweezers Combined With Single-Molecule Confocal Microscopy. Meth. Enzymol. 582, 137–169 (2017).
33. Righini, M. et al. Full molecular trajectories of RNA polymerase at single base-pair resolution. Proceedings of the National Academy of Sciences 115, 1286–1291 (2018).
34. Patrick, E. M., Srinivasan, S., Jankowsky, E. Comstock, M. J. The RNA helicase Mtr4p is a duplex-sensing translocase. Nat Chem Biol 13, 99–104 (2017).
35. Bustamante, C., Marko, J. F., Siggia, E. D., Smith, S. Entropic Elasticity of Lambda-Phage DNA. Science, 265, 1599-600 (1994).
36. Cluzel, P., Lebrun, A., Heller, C., Lavery, R., Viovy, J. L., Chatenay, D., Caron, F. DNA: An Extensible Molecule. Science, 271, 792-4 (1996).
37. Smith, S. B., Cui, Y., Bustamante, C. Overstretching B-DNA: The Elastic Response of Individual Double-Stranded and Single-Stranded DNA Molecules. Science, 271, 795-9 (1996).
38. Sgouralis, I., Whitmore, M., Lapidus, L., Comstock, M. J. Pressé, S. Single molecule force spectroscopy at high data acquisition: A Bayesian nonparametric analysis. J Chem Phys 148, 123320 (2018).
39. Dai, J., Carver, M., Punchihewa, C., Jones, R. A. Yang, D. Structure of the Hybrid-2 type intramolecular human telomeric G-quadruplex in K+ solution: insights into structure polymorphism of the human telomeric sequence. Nucleic Acids Res 35, 4927–4940 (2007).

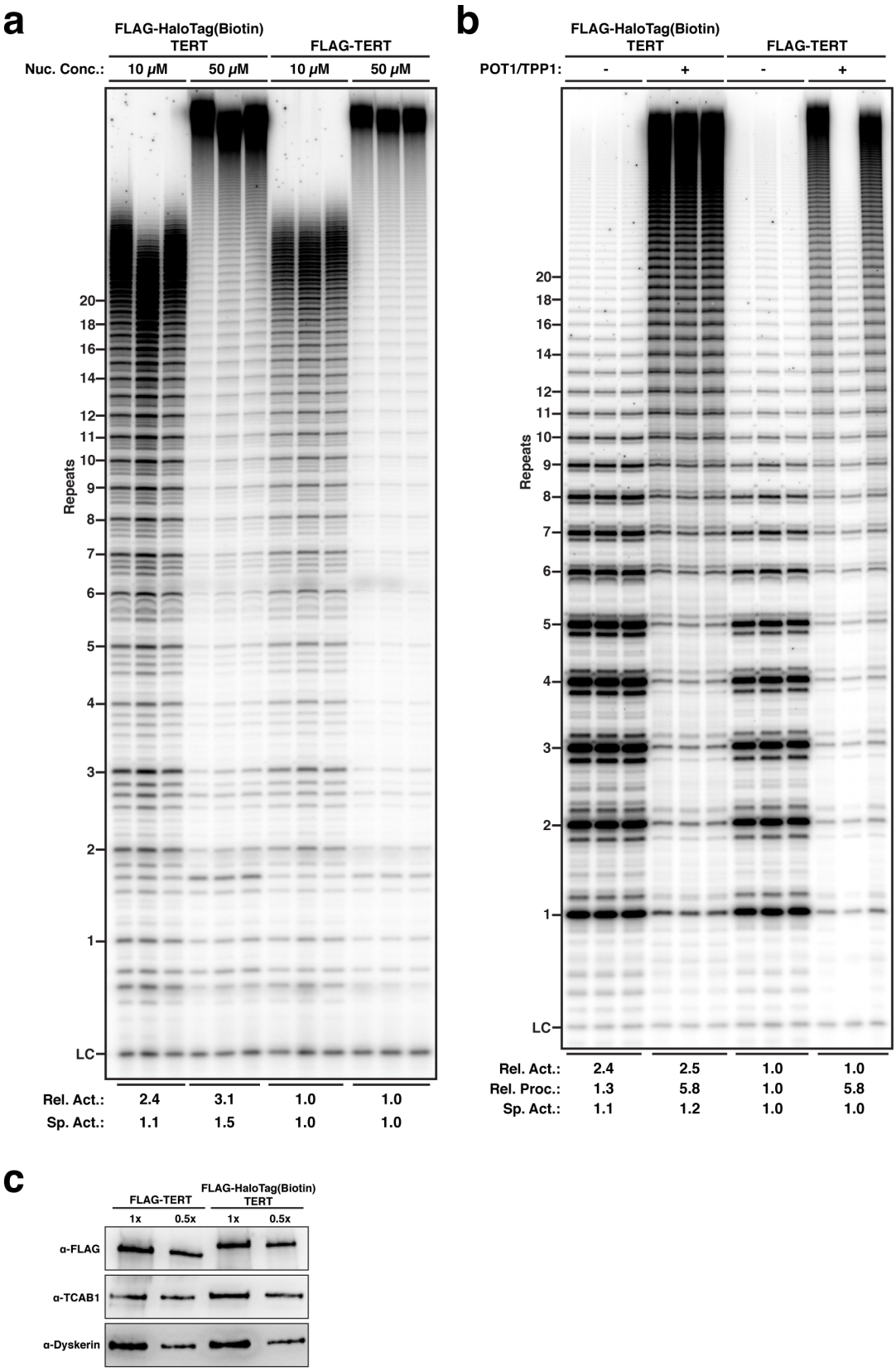

Extended Data Figure 1. The 3xFLAG-HaloTag on TERT modified with biotin does not affect telomerase activity, processivity, and stimulation by POT1/TPP1. a, Direct telomerase primer extension assay of 3xFLAG-HaloTag-TERT modified with biotin and 3xFLAG-TERT containing telomerase in reaction buffer containing 10 μM or 50 μM dNTPs and 50 mM KCl (LC = loading control). Relative activity is total lane intensity normalized to LC and the respective 3xFLAG-TERT telomerase activity. Specific activity is additionally normalized to the relative amount of TR (Fig. 1d). **b**, Direct telomerase primer extension assay of 3xFLAG-HaloTag-TERT modified with biotin and 3xFLAG-TERT containing telomerase in the absence and presence of POT1/TPP1 in buffer containing 150 mM KCl. Relative activity is total lane intensity normalized to LC and the respective 3xFLAG-TERT telomerase activity. Specific activity is additionally normalized to the relative amount of TR (Fig. 1d). Processivity is calculated by dividing the intensity of products greater than 6 repeats by total lane intensity. **c**, Western blot of purified 3xFLAG- and 3xFLAG-HaloTag-TERT containing telomerase samples, probed with anti-FLAG-M2-HRP (top), TCAB1 (middle), and dyskerin (bottom) antibodies.

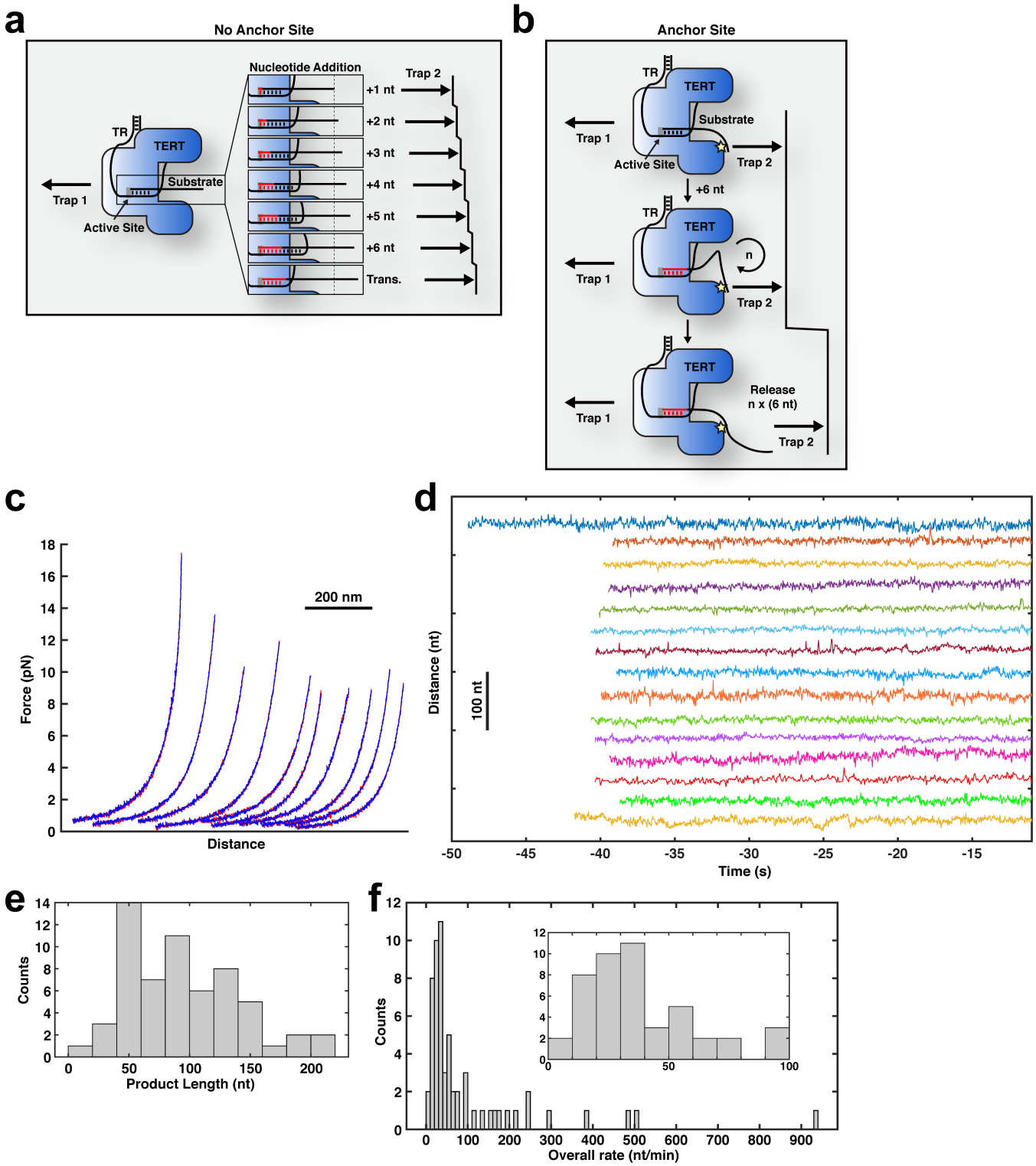

Extended Data Figure 2. Telomerase tethers are stable in the absence of nucleotides and elongate in the presence of nucleotides. **a**, Expected elongation step pattern of telomerase without anchor site function. **b**, Expected elongation step pattern of telomerase with anchor site function. **c**, Force-extension curves of tethers formed by telomerase and substrate showing measurements (red) and polymer model (blue). **d**, Representative time trajectories (30 ms per data point) of telomerase catalysis prior to transfer into dNTP containing buffer. **e**, Distribution of total tether elongation by telomerase (n = 60 traces). **f**, Distribution of overall elongation rate for all telomerase elongation trajectories (n = 60 traces).

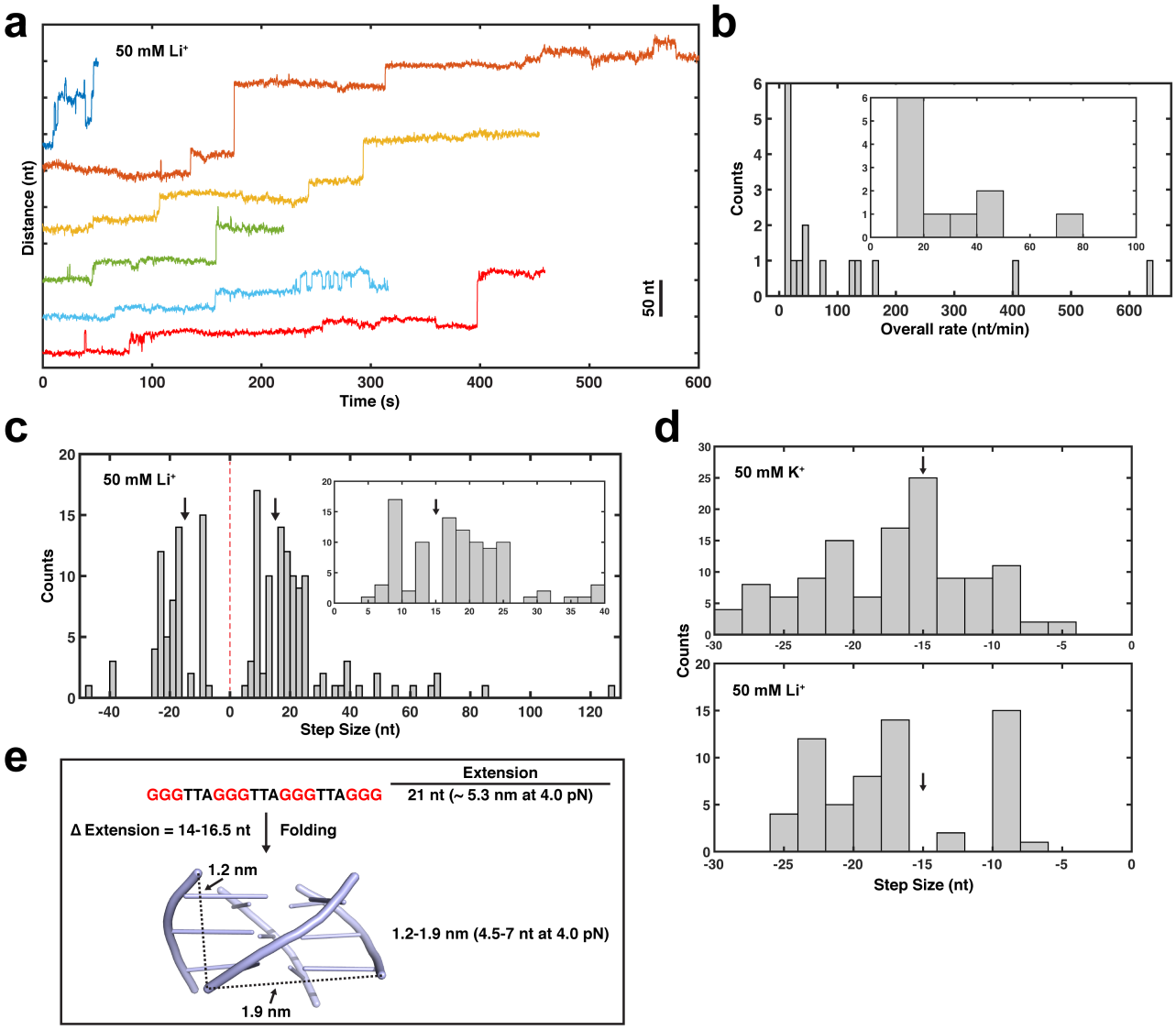

Extended Data Figure 3. Analysis of telomerase catalysis in the presence of LiCl. **a**, Representative time trajectories (120 ms per data point) of telomerase catalysis in reaction buffer containing 50 mM LiCl after transfer into dNTP containing buffer (t = 0). **b**, Distribution of overall elongation rate in the presence of 50 mM LiCl for all telomerase elongation trajectories (n = 16 traces). **c**, Distribution of the step sizes of telomerase trajectories in reaction buffer containing 50 mM LiCl (n = 16 traces, 171 steps). **d**, Distribution of reverse step sizes of telomerase trajectories in reaction buffer containing 50 mM KCl (n = 60 traces, top) and 50 mM LiCl (n = 17 traces, bottom). **e**, Expected extension change for the formation of a G-quadruplex structure formed by four TTAGGG repeats (PDB: 2JPZ [39] only showing the deoxyguanosine monophosphates). Expected measured change in extension is the difference between the average extension of the unfolded 21 nt of ssDNA polymer, and the average extension of the folded GQ structure measured from the 5'-to-3' termini. Distances (dashed lines) indicate the minimal (1.2 nm) and maximal (1.9 nm) 5'-to-3' distances of possible G-quadruplex topologies.

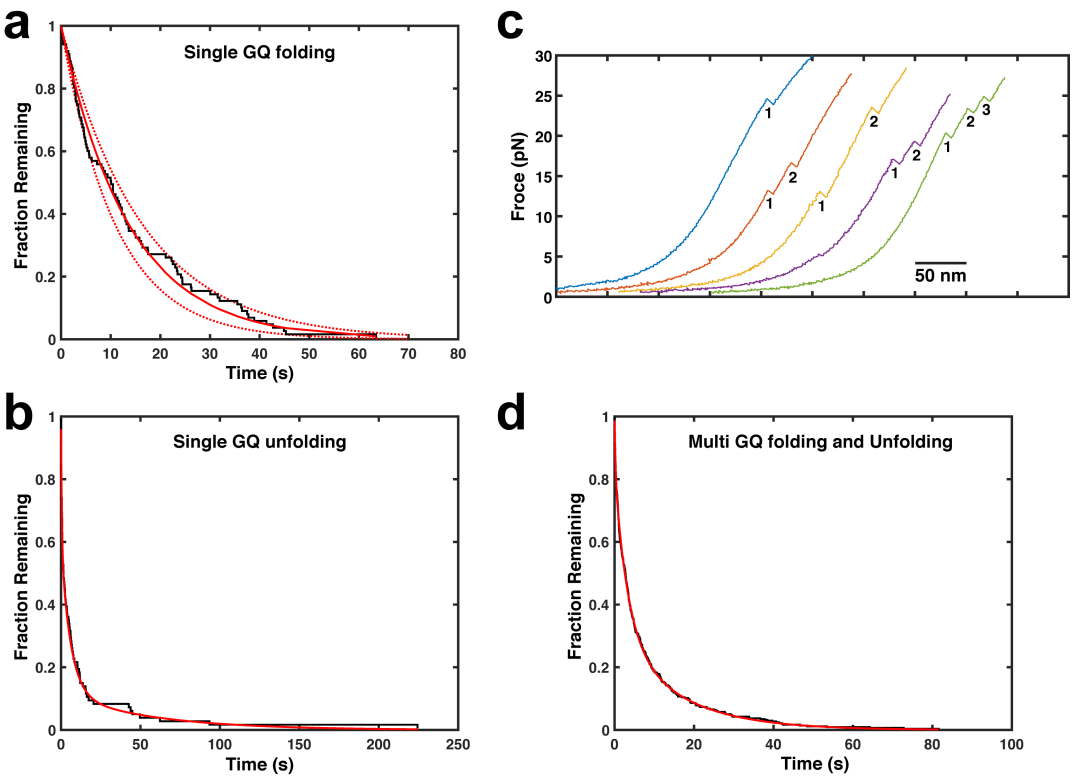

Extended Data Figure 4. Analysis of G-quadruplex formation using high-resolution optical tweezers. a, Inverse cumulative distribution of dwell times for folding steps of single GQ tethers (black staircase, n = 9 tethers, 94 dwell times). Solid red line indicates a single exponential fit, dashed lines the 90% confidence intervals. **b**, Inverse cumulative distribution of dwell times for unfolding steps of single GQ tethers (black staircase, n = 9 tethers, 90 dwell times). Solid red line indicates fit to the sum of three exponential decays (τ_{u1}=0.51±0.13, τ_{u2}=6.0±1.7, and τ_{u3}=56±33 s, weights of 41±8%, 47±9% and 12±6%). **c**, Force extension curves of $(TTAGGG)_{12}$ tethers. Numbers mark unfolding events. **d**, Inverse cumulative distribution of dwell times for folding and unfolding steps of multi GQ tethers (black staircase, n = 5 tethers, 389 dwell times). Solid red line indicates fit to the sum of three exponential decays (τ_1=0.23±0.12, τ_2=3.3±0.8, and τ_3=15±3 s, weights of 17±5%, 52±7% and 31±8%).

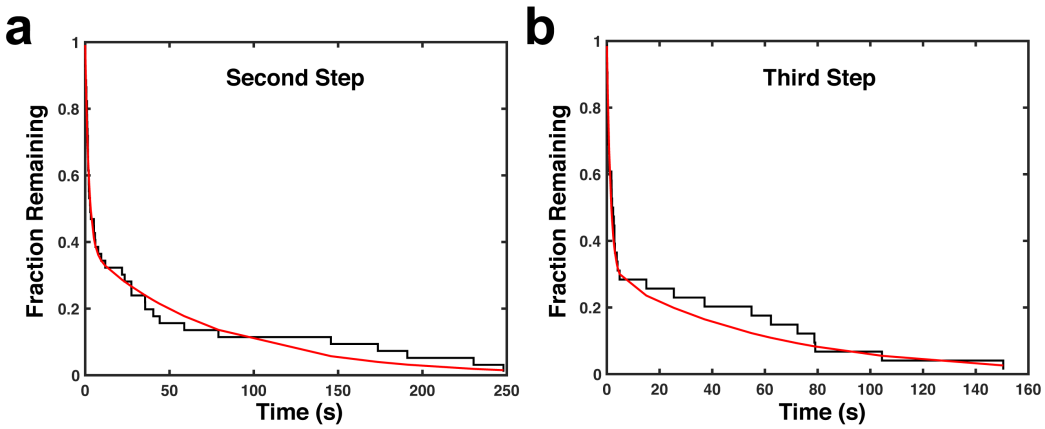

Extended Data Figure 5. Dwell time analysis of the second and third transition of all telomerase trajectories. a, Inverse cumulative distribution of dwell times for the second transition of all telomerase trajectories (n = 60 traces). Solid red line indicates fit to the sum of two exponential decays. **b**, Inverse cumulative distribution of dwell times for the third transition of all telomerase trajectories (n = 60 traces). Solid red line indicates fit to the sum of two exponential decays.

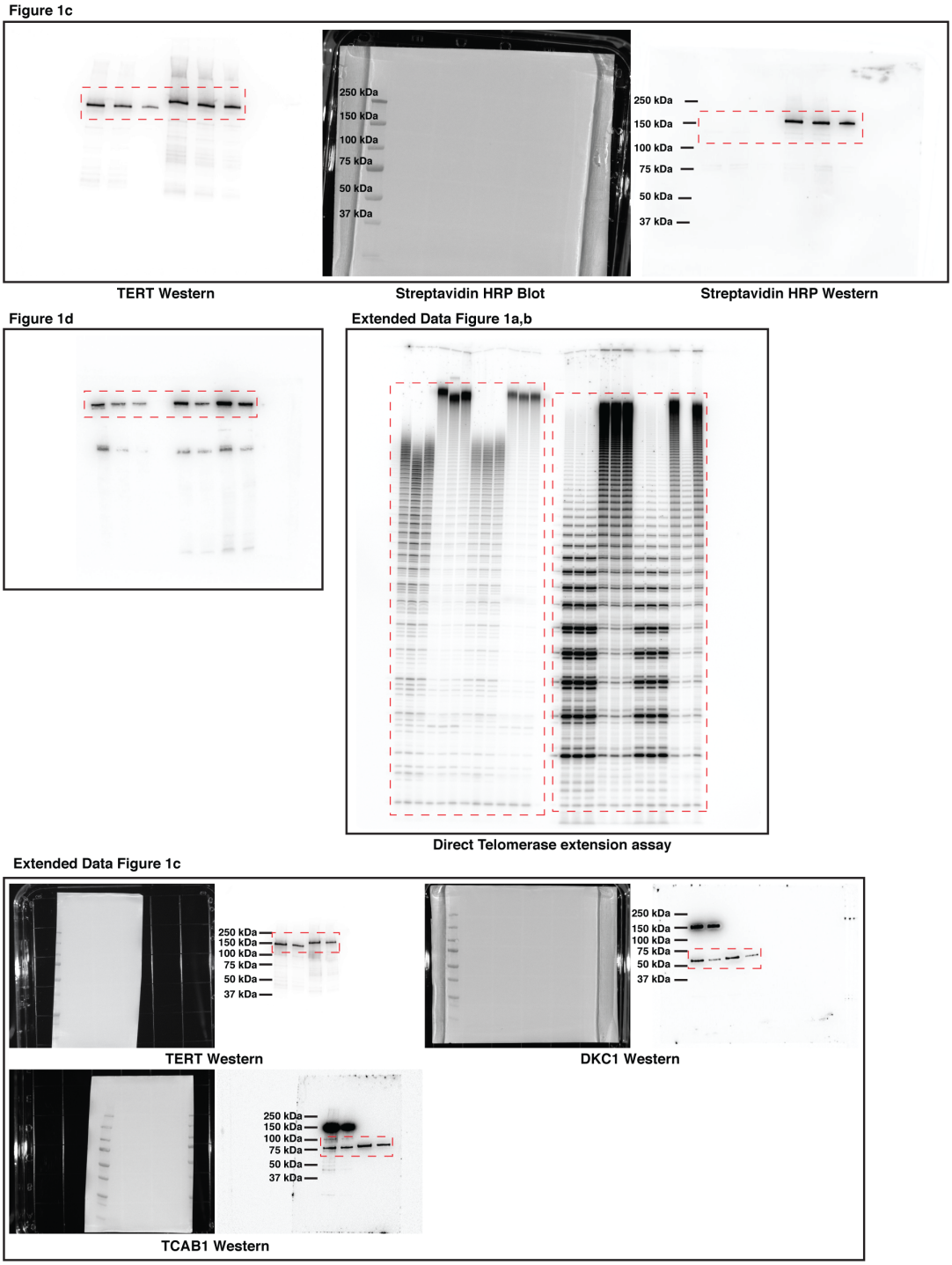

Supplementary Figure 1. Unedited gel images for all data presented in this manuscript.

Name	Sequence
Substrate Handle Oligo 1	TGGCGACGGCAGCGAGGCTTTTTTTTTTTTTTTTT TTTTTTTTTTTTTTTTGGGTTAGGGTTAGGG
Substrate Handle Oligo 2	AAAAAAAAAAAAAAAAGCCTCGCTGCCGTCGCCA/3Dig_N/
Biotin-Dig Handle Oligo 1	/5Biosg/TGGTCTTCGGTTTCCGTGTT
Biotin-Dig Handle Oligo 2	/5DigN/CAACAACGTTGCGCAAACT
TR Probe 1	CTCCAGGCGGGGTTCGGGGGCTGGGCAG
TR Probe 2	CTTTTCCGCCCGCTGAAAGTCAGCGAG
TR Probe 3	CATGTGTGAGCCGAGTCCTGGGTGCACG
Primer A	TTAGGGTTAGGGTTAGGG
Primer A5	TTAGGGTTAGCGTTAGGG
Primer A-2	TTAGGGTTAGGGTTAG
GGG(TTAGGG)3	/5Phos/CCTGGAGGACTTGTTTTTAGGGTTAGGG TTAGGGTTAGGGTTCAGTATCGACCCACTGGC
FRET Donor	/5Cy3/ACAAGTCCT
FRET Acceptor	/5Phos/TCGATACTG/3Cy5Sp/
(TTAGGG)12	/5Phos/AGCTTTTTAGGGTTAGGGTTAGGGTTAGGGTTAGGG TTAGGGTTAGGGTTAGGGTTAGGG TTAGGGTTAGGGTTAGGGTTCCCACTGGC
pBR322 for	/5Biosg/TGAAGTGGTGGCCTAACTACG
pBR322 rev	TTGCATGATAAAGAAGACAGTCAT
Lambda for	/5DigN/GGGCAAACCAAGACAGCTAA
Lambda rev	CCCGTCATACACTTGCTCCT

Supplementary Table 1. Oligonucleotides used in this study.